Functional relationships between denudation and hillslope form and relief

Joshua J. Roering [a,*], J. Taylor Perron [b], James W. Kirchner [c]

[a] Department of Geological Sciences, University of Oregon, Eugene, OR 97403-1272, United States
[b] Department of Earth and Planetary Sciences, Harvard University, Cambridge, MA 02138, United States
[c] Department of Earth and Planetary Science, University of California, Berkeley, Berkeley, CA 94720-4767, United States

Abstract

Functional relationships between landscape morphology and denudation rate allow for the estimation of sediment fluxes using readily available topographic information. Empirical studies of topography-erosion linkages typically employ data with diverse temporal and broad spatial scales, such that heterogeneity in properties and processes may cloud fundamental process-scale feedbacks between tectonics, climate, and landscape development. Here, we use a previously proposed nonlinear model for sediment transport on hillslopes to formulate 1-D dimensionless functions for hillslope morphology as well as a generalized expression relating steady-state hillslope relief to erosion rate, hillslope transport parameters, and hillslope length. For study sites in the Oregon Coast Range and Gabilan Mesa, CA, model predictions of local relief and average hillslope gradient compare well with values derived from high-resolution topographic data acquired via airborne laser altimetry. Our formulation yields a nondimensional number describing the extent to which the nonlinearity in our gradient-flux model affects slope morphology and landscape response to tectonic and climatic forcing. These results should be useful for inferring rates of hillslope denudation and sediment flux from topography, or for coarse-scale landscape evolution simulations, in that first-order hillslope properties can be calculated without explicit modeling of individual hillslopes.
© 2007 Elsevier B.V. All rights reserved.

Keywords: relief; hillslope; erosion; landscape; rock uplift

1. Introduction

Morphologic characteristics of hillslopes, such as average slope angle and channel-to-divide relief, reflect complex feedbacks between tectonic forcing and climate-dependent erosional processes. Intuitively, most geomorphologists understand that erosion rates should increase with terrain steepness and in fact several equations have been proposed to quantify how denudation varies with different measures of topographic inclination (Aalto et al., 2006; Ahnert, 1970; Granger et al., 1996; Montgomery and Brandon, 2002; Summerfield and Nulton, 1994). Early studies focused on continental and orogen-scale topography, using topographic maps to estimate mean local relief (which serves as a surrogate for mean slope) (Ahnert, 1970; Milliman and Syvitski, 1992; Pinet and Souriau, 1988). The seminal paper by Ahnert (1970) proposed systematic relief-denudation coupling in mid-latitude drainage

* Corresponding author. Tel.: +1 541 346 5574; fax: +1 541 346 4692.
E-mail addresses: jroering@uoregon.edu (J.J. Roering),
perron@eps.harvard.edu (J.T. Perron), kirchner@berkeley.edu
(J.W. Kirchner).

basins by showing that denudation varies proportionally with mean local relief, attaining a maximum value of ~ 0.45 mm yr^{-1} as relief approaches 3000 m.

More recent studies have used digital elevation models (DEMs) to measure topographic characteristics, and thermochronometry or isotopic methods to quantify long-term exhumation rates in tectonically active, mountainous areas (Aalto et al., 2006; Granger et al., 1996; Montgomery and Brandon, 2002; Binnie et al., 2007). Several of these analyses suggest that in steep terrain, denudation rates increase rapidly while slope angles remain relatively constant, such that topographic relief becomes effectively decoupled from erosion rate via accelerated mass wasting (Montgomery and Brandon, 2002; Binnie et al., 2007; Burbank et al., 1996). Data compiled for tectonically active regions suggests that erosion rate increases rapidly (up to ~ 9 mm yr^{-1}) as mean local relief approaches 1500 m (Montgomery and Brandon, 2002). This highly nonlinear denudation-relief relationship diverges from the linear trend proposed by Ahnert (1970) and supports the notion that hillslope angles may approach a limiting value despite further increases in erosion rate via baselevel lowering (Strahler, 1950; Penck, 1953; Carson and Petley, 1970).

The attainment of an effectively decoupled denudation-relief condition may be reflected by steep mean hillslope angles with low dispersion (Strahler, 1950; Montgomery, 2001). The hillslope angle that defines the geomorphic limit to topographic relief, however, may be highly variable due to climatic, lithologic, or other environmental factors (Strahler, 1950; Montgomery, 2001; Roering et al., 2005; Schmidt and Montgomery, 1995; Carson, 1976; Freeze, 1987). Nonetheless, a recent study in the San Bernardino Mountains, Southern California (Binnie et al., 2007), shows a highly nonlinear denudation-slope relationship strikingly similar to one generated in the Olympic Mountains, Washington (Montgomery and Brandon, 2002). This correspondence may reflect a similar process transition at both sites whereby disturbance-driven transport and erosion on gentle slopes varies linearly with gradient and detachment-limited processes (such as slope instability) drive rapid denudation as slopes steepen (Binnie et al., 2007). A theoretical basis for this continuous process transition is lacking and the extent to which these two process regimes overlap remains unclear. Because the distribution and intensity of geomorphic processes in a particular landscape can be diverse, the combined impact of soil transport, shallow landslides, deep-seated landslides, debris flows, and fluvial and/or glacial incision may generate a distribution of local relief values characteristic of that setting. The extent to which environmental and

geologic factors influence denudation-slope relationships has primarily been addressed for large catchments (Milliman and Meade, 1983).

Morphologic measures used to predict denudation rate (e.g., local relief and average gradient) are typically calculated over spatial scales (1–10 km) that are much larger than the scale of individual hillslopes ($\ll 1$ km). As a result, these morphologic measures inevitably fuse the signatures of valley-forming and hillslope processes, making it difficult to quantify the relative importance of different relief-generating mechanisms. Alternatively, one can derive theoretical formulations of relief-denudation relationships from the mechanics of individual relief-generating processes that occur in mountainous areas (e.g., debris flows (Stock and Dietrich, 2003) and bedrock channel incision (Whipple et al., 1999)). Here, we follow this approach, focusing on soil-mantled hillslopes and their contribution to local relief. We present a simplified, one-dimensional, analytical solution for steady-state hillslope profiles, as well as their slope, curvature, and overall relief, based on a previously published nonlinear hillslope erosion model (Andrews and Bucknam, 1987; Roering et al., 1999). Our formulation results in a single function describing how hillslope relief varies with erosion rate, hillslope length, disturbance energy that drives sediment transport, and the critical hillslope angle. This relief function yields predictions that are consistent with measurements of erosion rates (using cosmogenic radionuclides) and landscape morphology (using airborne laser altimetry) at sites in California and Oregon. Our findings provide a straightforward means of gauging landscape sensitivity to changes in tectonics and climate and should be useful for inferring process rates from high-resolution topography. This conceptual framework may also be useful for embedding sub-grid scale slope morphology within grid cells of coarse-scale landscape evolution models.

2. Steady-state model for hillslope morphology and relief

Models representing sediment transport on hillslopes generally incorporate a slope dependency, such that flux rates increase with local slope (Anderson, 1994; Howard, 1994). As slope angles approach the angle of repose, frictional resistance to transport decreases with the result that incremental increases in slope can produce large increases in sediment flux. At angles near the critical value, mass wasting may also ensue, further contributing to rapid fluxes. Predictions from so-called "nonlinear transport" models are consistent with topographic, field, and experimental findings (Roering

et al., 1999; Gabet, 2000, 2003; Roering and Gerber, 2005; Roering et al., 2001a). Here, we use a nonlinear transport equation originally proposed by Andrews and Bucknam (1987) and reformulated by Roering et al. (1999), which states that sediment flux, q_s, varies with hillslope gradient, ∇z, according to

$$\widetilde{q}_s = \frac{-K\nabla z}{1 - (|\nabla z|/S_c)^2} \tag{1}$$

where K is a transport coefficient reflecting the power expenditure of soil disturbance mechanisms ($L^2 T^{-1}$) and S_c is the critical hillslope gradient at which downslope sediment fluxes become infinite. Other nonlinear models have recently been proposed whereby soil transport rates vary with soil depth (Mudd and Furbish, 2005; Heimsath et al., 2005; Furbish and Fagherazzi, 2001). These models have utility in low-relief settings and offer an opportunity to link soil transport with ecological processes (Yoo et al., 2005), but they do not account for the rapid increases in flux on steep slopes that lead to the development of roughly planar threshold landscapes. A recently proposed revision of Eq. (1) (which stipulates that K varies nonlinearly with soil depth) has important implications for local-scale slope morphology (Roering, 2006), but does not affect modeled values of hillslope relief and average gradient which are the focus of this contribution.

We use a one-dimensional (i.e. profile) analysis that does not include a description of channel formation via processes such as debris flows or fluvial incision. Thus, our model does not describe the evolution of ridge-and-valley topography through the combined action of hillslope transport and channel-forming processes, but it is sufficient to describe hillslopes whose length scale is defined by the typical distance particles travel before entering the valley network. To quantify the implications of nonlinear transport for morphology-denudation linkages, we combine a one-dimensional version of Eq. (1) with the continuity equation, obtaining:

$$\rho_s \frac{\partial z}{\partial t} = -\rho_s \frac{\partial}{\partial x}\left(\frac{-K(\partial z/\partial x)}{1 - [(\partial z/\partial x)/S_c]^2}\right) + \rho_r U \tag{2}$$

where z is elevation (L), t is time, x is horizontal distance (L), ρ_r and ρ_s are densities of rock and soil (M L^{-3}), respectively, and U is rock uplift rate ($L T^{-1}$). Assuming steady-state denudation ($\partial z/\partial t \rightarrow 0$) such that the rate of erosion of the bedrock surface, E, equals the rate of rock uplift, U, Eq. (2) can be differentiated and re-arranged to produce an expression describing how curvature, C,

tends toward zero (planar slopes) as hillslope gradients approach the critical value, S_c:

$$C = \frac{d^2 z}{dx^2} = \left(\frac{-(\rho_r/\rho_s)E}{K}\right)\frac{\left(1 - \left(\frac{dz/dx}{S_c}\right)^2\right)^2}{1 + \left(\frac{dz/dx}{S_c}\right)^2} \tag{3}$$

Note that $C = d^2z/dx^2$ is defined such that it takes on negative values for conventional, convex-upward hillslopes. At hilltops (where $dz/dx \rightarrow 0$), Eq. (3) reduces to only its leading term, which can be re-arranged to solve for the soil transport coefficient, K, given estimates of hilltop curvature, C_{HT}, and erosion rate, E:

$$K = \frac{(\rho_r/\rho_s)E}{-C_{HT}} \tag{4}$$

Substituting Eq. (4) into Eq. (3) yields an expression for curvature variations given estimates of hilltop curvature and the critical gradient S_c:

$$C = C_{HT}\frac{\left(1 - \left(\frac{dz/dx}{S_c}\right)^2\right)^2}{1 + \left(\frac{dz/dx}{S_c}\right)^2} \tag{5}$$

Eq. (5) indicates that curvature attains its maximum value at the hilltop, and expresses how rapidly curvature decreases away from the hilltop, as S approaches S_c.

Eq. (3) can be written as a first-order ordinary differential equation in dz/dx. Solving this equation and applying the boundary condition $dz/dx = 0$ at $x = 0$ yields the following expression for slope (here, the absolute value of the gradient):

$$S = |\frac{dz}{dx}| = \frac{KS_c^2}{2(\rho_r/\rho_s)E|x|}\left(\sqrt{1 + \left(\frac{2(\rho_r/\rho_s)Ex}{KS_c}\right)^2} - 1\right) \tag{6}$$

where $x = 0$ is the hilltop (such that $dz/dx \rightarrow 0$ as $x \rightarrow 0$). Eq. (6) predicts that gradient values increase nonlinearly, approaching the critical gradient S_c on hillslopes that are sufficiently long. Integrating Eq. (6) yields an expression for the steady-state hillslope elevation profile,

$$z = \frac{KS_c^2}{2(\rho_r/\rho_s)E}\left[\ln\left(\frac{1}{2}\left(\sqrt{1 + \left(\frac{2(\rho_r/\rho_s)Ex}{KS_c}\right)^2} + 1\right)\right) - \sqrt{1 + \left(\frac{2(\rho_r/\rho_s)Ex}{KS_c}\right)^2} + 1\right] \tag{7}$$

where the constant of integration has been defined such that $z=0$ at $x=0$. Eqs. (3), (6) and (7) can be combined, simplified, and rewritten in dimensionless form, as functions of just two variables: a dimensionless erosion rate $E^*=E/E_R$, where the 'reference' erosion rate E_R is defined as $E_R=KS_c/(2L_H(\rho_r/\rho_s))$ and a dimensionless distance $x^*=x/L_H$, where L_H is the hillslope length (measured horizontally from the hilltop to the channel margin):

$$C^*=-C\frac{L_H}{S_c}=\frac{E^*}{\sqrt{1+(E^*x^*)^2}} \qquad (8a)$$
$$-\frac{1}{E^*(x^*)^2}\left(\sqrt{1+(E^*x^*)^2}-1\right)$$

$$S^*=\frac{S}{S_c}=\frac{1}{(E^*x^*)}\left(1-\sqrt{1+(E^*x^*)^2}\right) \qquad (8b)$$

$$z^*=\frac{z}{S_cL_H}=\frac{1}{E^*}\left[\begin{array}{l}\ln\left(\frac{1}{2}\left(1+\sqrt{1+(E^*x^*)^2}\right)\right)\\[2mm]+1-\sqrt{1+(E^*x^*)^2}\end{array}\right]. \qquad (8c)$$

Eqs. (8a) (8b) (8c) predict the morphology of steady-state hillslopes, including the expected degree of hillslope relief development, given knowledge of hillslope length, erosion rate, and transport parameters (Fig. 1). The ratio $x^*=x/L_H$ (which varies between −1 and 1) represents relative position along the hillslope where $x/L_H=0$ is the hilltop and $x/L_H=1$ and $x/L_H=-1$ correspond to hillslope-channel margins. The reference erosion rate E_R is the erosion rate that would steepen a hillslope of length L_H sufficiently such that at $x=L_H$, its gradient would equal $\sqrt{2}-1=0.414$ times the critical slope S_c (the 0.414 factor follows from the form of Eq. (7)). The dimensionless erosion rate E^* thus quantifies how base-level forcing interacts with the nonlinearity in our transport model (Eq. (1)) to regulate relief and hillslope morphology. For example, when the erosion rate, E, is slow compared to E_R ($E^*<1$), slopes are approximately parabolic (Fig. 1A), such that gradient increases approximately linearly with distance from the divide (Fig. 1B) and curvature values are relatively invariant (Fig. 1C). When erosion rates are fast compared to E_R ($E^*>1$), hillslope gradients approach the critical value downslope ($S/S_c\rightarrow1$), curvature values approach zero, and the hillslope profile approximates an angle-of-repose slope (Fig. 1A–C). The greater the erosion rate E compared to the reference value E_R (and thus the greater the dimensionless value E^*), the smaller
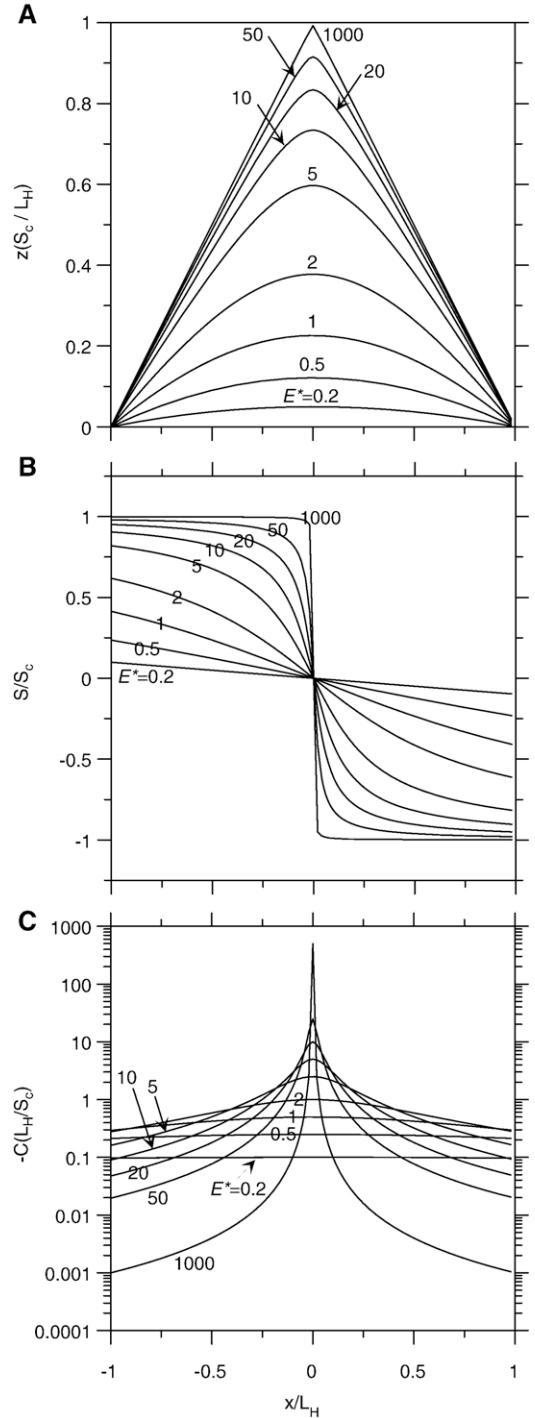

Fig. 1. Nondimensional profiles of hillslope elevation (A), gradient (B), and curvature (C), calculated from Eq. (8a), (8b) and (8c). The ratio x/L_H reflects relative position along hillslopes and $E^*=E/E_R$ or $E^*=(2C_{HT}L_H)/S_c$, where $E_R=KS_c/(2L_H(\rho_r/\rho_s))$. At higher values of E^*, the nonlinearity in our transport model (Eq. (1)) becomes increasingly influential in shaping hillslope morphology, such that gradients approach the critical value and curvature becomes increasingly focused at the crest, with increasingly planar sideslopes (curvature near zero).

the fraction of the hillslope length (i.e., the smaller the range of x^*) over which the hillslope is approximately parabolic, and the larger the range of x^* over which it is nearly planar. Thus, these equations provide a framework for predicting how variations in base-level forcing or transport parameters will affect hillslope morphology — or, alternatively, for using hillslope morphology to infer how base-level forcing and/or transport parameters vary across a landscape.

To clarify the relationship between hillslope relief and denudation rate, Eq. (8c) can be manipulated to obtain a dimensionless relief function. First, recall that hillslope relief, R, can be defined as:

$$R = z(0) - z(L_H) \tag{9}$$

Hillslope relief can be intuitively expressed in dimensionless form by taking its ratio with respect to $R_{max} = S_c L_H$, the greatest possible relief for a hillslope of length L_H. Thus, the dimensionless relief number R^* can be interpreted either as the ratio of R to R_{max}, or as the ratio of the mean slope ($\bar{S} = R/L_H$) to the critical slope S_c; the two quantities are formally equivalent. Combining Eqs. (8c) and (9), the dimensionless relief number R^* can be calculated as:

$$R^* = \frac{R}{S_c L_H} = \frac{\bar{S}}{S_c} = \frac{1}{E^*}$$
$$\left(\sqrt{1 + (E^*)^2} - \ln\left(\frac{1}{2}\left(1 + \sqrt{1 + (E^*)^2}\right) \right) - 1 \right) \tag{10}$$

Using Eq. (4), we can recast the dimensionless erosion number as $E^* = (-2C_{HT}L_H)/S_c$. As shown in Fig. 2, Eq. (10) states that for E^* values of order 1 or less, hillslope profiles are nearly parabolic and R^* increases approximately proportionally to erosion rate; in the limit of small E^*, $R^* \approx E^*/4$. As E^* rises above 1, R^* becomes progressively less sensitive to erosion rates, with hillslope profiles becoming increasingly planar near the critical gradient S_c, and convexity becoming increasingly localized near the ridge crest. This analysis indicates that the transition between landscapes that are morphologically sensitive and insensitive to changes in erosion rate is continuous, consistent with empirical findings (Montgomery and Brandon, 2002; Binnie et al., 2007), but in contrast to the notion that a discrete threshold defines these two regimes (Burbank et al., 1996; Carson and Petley, 1970; Hutchinson, 1967). As such, Fig. 2 provides a quantitative framework for evaluating the degree of erosion-relief coupling in hilly and mountainous landscapes.

3. Study sites: Oregon Coast Range and Gabilan Mesa

To test the utility of our denudation-relief formulation, we compared model predictions of average slope gradient and hillslope relief to measurements in two well-studied landscapes, the Oregon Coast Range and Gabilan Mesa, Central California (Fig. 3). Both sites are exceptional natural laboratories for studying process-form linkages. Previous work at both sites has: 1) measured hillslope morphology using high-resolution topographic data acquired via airborne laser altimetry, 2) estimated erosion rates via cosmogenic radionuclides, and 3) calibrated transport parameters (K and S_c) that are used in the analysis presented above. Previous work has also shown that both sites approximate an erosional steady state, based on erosion rate data and broadly consistent ridge-valley sequences with characteristic slope morphology. The characteristic morphology of the two sites is dramatically different, however, so they should occupy different regions within our relief-denudation formulation (Fig. 2). Oregon Coast Range slopes are steep and drainage divides are sharply defined, whereas Gabilan Mesa slopes have broader convexity and more gradual transitions into convergent zones (Fig. 3).
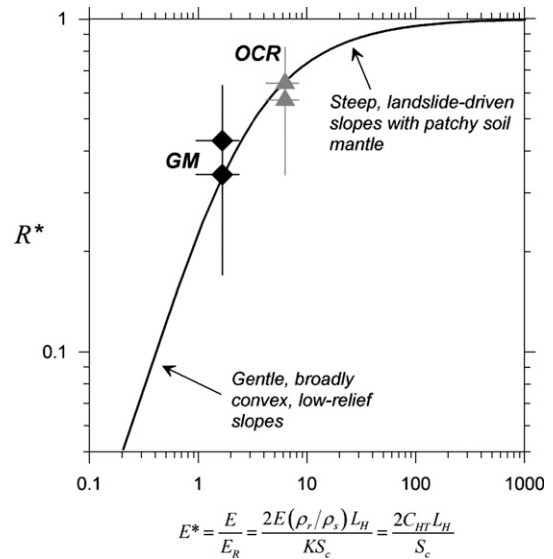

Fig. 2. Nondimensional relationship between relief (R^*) and erosion rate (E^*). For E^* of order 1 or less, relief increases approximately proportionally to erosion rate for any given hillslope length L_H. For higher values of E^*, slopes become increasingly planar near the critical gradient S_c, and thus relief becomes increasingly insensitive to changes in erosion rate or transport coefficient K, and instead depends only on S_c and the hillslope length L_H. R^* values for our OCR and GM study sites (plotted with gray triangles and black diamonds, respectively) are estimated using the equations $R^* = \bar{S}/S_c$ and $R^* = R/(L_H S_c)$, see Table 1 for calculation details.

Oregon Coast Range

Total relief = 320 m
Avg. slope gradient = 0.75
Avg. hillslope relief = 38 m
Area = 710 m x 600 m

★ OR

CA

★

Gabilan Mesa, California

Total relief = 120 m
Avg. slope gradient = 0.41
Avg. hillslope relief = 37 m
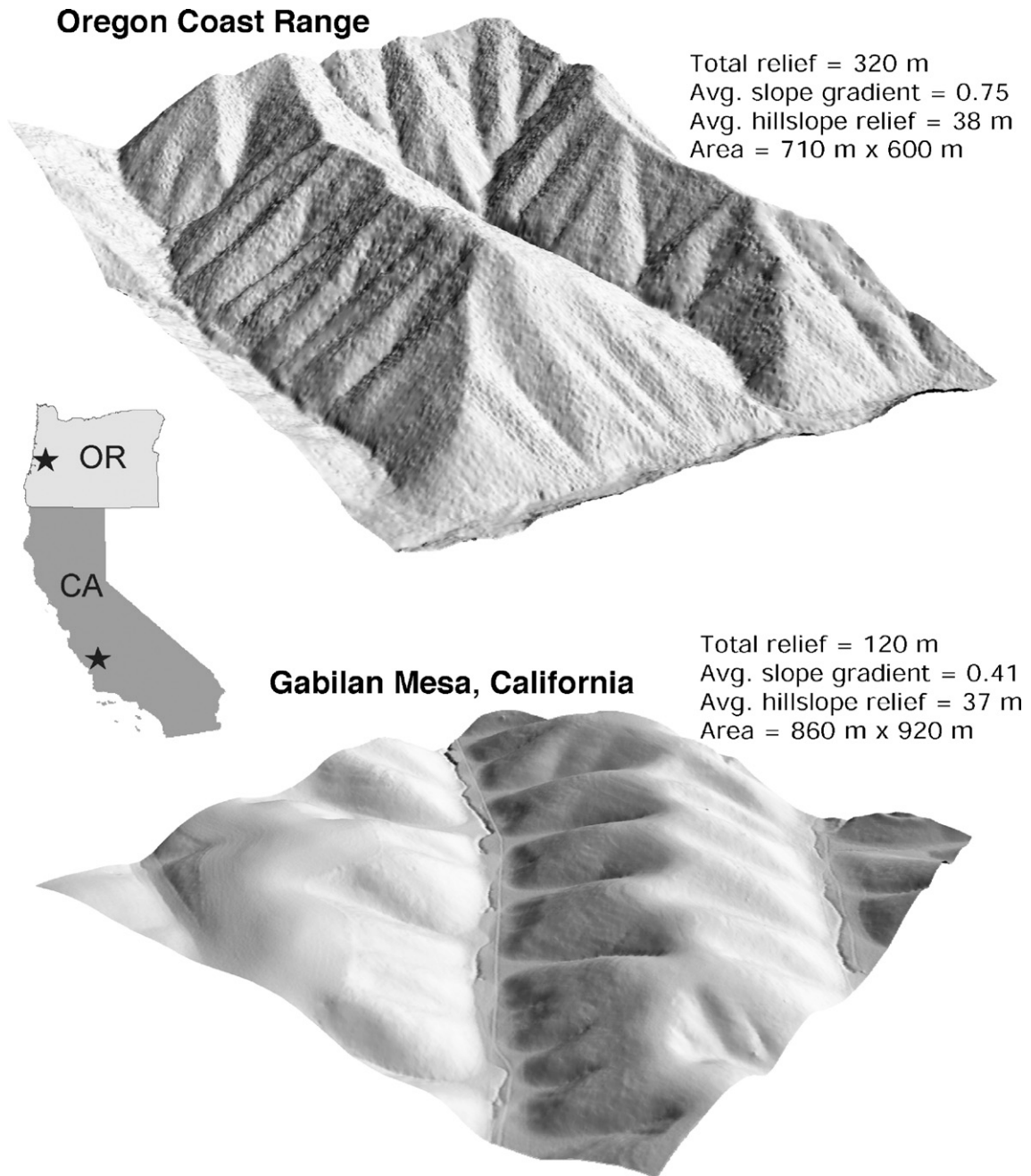Area = 860 m x 920 m

Fig. 3. Perspective shaded relief images of Gabilan Mesa (top) and Oregon Coast Range (bottom) study sites using high-resolution topographic data acquired via airborne laser altimetry. Steep, nearly planar slopes of the OCR contrast with the broad, convex GM slopes. Airborne laser altimetry data for our Mettman Ridge study area near Coos Bay, Oregon, was collected in 1996 by Airborne Laser Mapping, Inc. Airborne laser altimetry data for a 40 km² area of the GM near Bradley, California was collected in 2003 by the National Center for Airborne Laser Mapping (NCALM). Geographical coordinates for the GM and OCR sites are lat=35.893°, long=−120.726° and lat=43.463°, long=−124.119°, respectively. Axes in both images are in UTM (meters).

3.1. Oregon Coast Range

The Oregon Coast Range (OCR) is a humid, forested, mountainous landscape whose central and southern regions are underlain by a thick section of Eocene turbidites mapped as the Tyee Formation (Baldwin, 1956; Snavely et al., 1964). The Tyee Formation has been compressed into a series of low-amplitude, north–northeast striking folds

(Baldwin, 1956). The OCR is situated above a subduction zone and has experienced uplift over the last 20–30 Ma (Orr et al., 1992).

The topography of the OCR has been characterized as steep and highly dissected with relatively uniform ridge and valley terrain (Montgomery, 2001; Dietrich and Dunne, 1978; Reneau and Dietrich, 1991). Typically, soils are relatively thin (∼0.4 m) on hilltops and sideslopes and thicker (∼1–2 m) in unchanneled valleys; these unchanneled valleys, or 'hollows' act as preferential source areas for shallow landslides, which often initiate debris flows (Dietrich and Dunne, 1978; Heimsath et al., 2001; Montgomery et al., 2000; Schmidt, 1999). Most studies of decadal-to-millennial scale patterns of sediment production and delivery in the OCR have focused on the cyclic infilling and evacuation of soil in steep, convergent hollows (Benda and Dunne, 1997; Reneau and Dietrich, 1990). Erosion rates estimated from analyses of short-term (∼10 yr) and long-term (∼5000 yr) sediment yields are commonly 0.07 to 0.15 mm yr^{-1} (Reneau and Dietrich, 1991; Heimsath et al., 2001; Beschta, 1978; Bierman et al., 2001), consistent with rates of coastal uplift (Kelsey et al., 1996) and Holocene bedrock channel incision (Personius, 1995). Based on these estimates, here we use an average erosion rate of 0.1 mm yr^{-1}. The consistency of these rates has been used to argue that an approximate balance exists between rock uplift and erosion in the OCR, such that hillslope morphology may be relatively uniform with time (Montgomery, 2001; Roering et al., 1999; Reneau and Dietrich, 1991). Previous calculations suggest that the short, steep hillslopes depicted in Fig. 3 can rapidly (∼40 kyr) adjust their morphology to climatic or tectonic perturbations (Roering et al., 2001b), providing further justification for the assumption of steady state erosion in OCR locales with regularly spaced ridge-valley sequences. In this study, we used parameters characteristic of the OCR study site, estimated by Roering et al. (1999) from topographic data ($K = 0.003$ m^2 yr^{-1} and $S_c = 1.2$).

3.2. Gabilan Mesa, Central California

The Gabilan Mesa (GM) occupies a region roughly 110 km long and 20 km wide on the eastern side of Central California's Salinas River Valley. Bounded by the Salinas River to the west and the San Andreas rift valley to the east, the GM consists of Pliocene shallow marine sediments of the Pancho Rico Formation overlain by Plio-Pleistocene subaerial sediments of the Paso Robles Formation (Dibblee, 1979; Dohrenwend, 1979a; Durham, 1974; Galehouse, 1967). Beginning in the late Pleistocene, incision of the Salinas River and uplift and southwestward tilting associated with transpression along the Rinconada–Reliz fault zone led to dissection of the GM by NE–SW trending valleys with orthogonal tributaries (Dibblee, 1979; Dohrenwend, 1979b). Parts of the original mesa surface remain undissected in a few locations, but most of the landscape has eroded well below this surface (Dohrenwend, 1979b).

The Salinas Valley's Mediterranean climate and strongly seasonal precipitation support an oak savannah ecosystem. Hillslope erosion is dominated by biogenic disturbance, including ground squirrel burrowing and tree throw, with a secondary contribution from overland flow. Valleys are episodically scoured by gullying that evacuates stored colluvium and erodes the underlying bedrock. Evidence of landsliding is rare. Soils are typically less than 1 m thick on ridgelines and thicker in valleys.

The long-term erosion rate in the GM can be constrained by dating the remnant portions of the original mesa surface (not shown in Fig. 3). Using surface exposure and burial ages measured from cosmogenic radionuclides in quartzite clasts in the Paso Robles Formations, Perron et al. (2005) and Perron (2006) estimated a surface age of 225+239/−139 kyr. The major valleys draining the GM in our study area have eroded 80±1 m below the original surface during this interval, implying a long-term erosion rate of 0.36+0.38/−0.22 mm yr^{-1}.

We can use this erosion rate and the form of the hillslopes to evaluate the closeness of the GM topography to equilibrium and to infer the value of K. Where $|dz/dx| \ll S_c$, such as on hilltops, K can be calculated using Eq. (4). The highly uniform hilltop curvature, C_{HT}, of -0.014 ± 0.0002 m^{-1} (S.D.=0.003 m^{-1}) on ridgelines in the GM with $dz/dx < 0.05 S_c$ suggests that the hillslopes may be in approximate topographic steady state. Further evidence of equilibrium topography is the remarkably uniform spacing of first-order valleys throughout the GM (Fig. 3) (Perron, 2006; Perron et al., 2003). Modeling of long-term landscape evolution indicates that valley spacing becomes more periodic as a landscape approaches topographic steady state (Perron et al., 2005; Perron, 2006). With $\rho_r/\rho_s = 1.5$ and the values of E and C_{HT} reported above, Eq. (4) yields $K = 0.038 + 0.040/−0.024$ m^{2}yr^{-1}. S_c has not been measured for the GM, and is here assumed to be 1.2, equal to the value inferred for the OCR. Because S_c does not typically differ from unity by more than a factor of 1.5, the impact of this approximation on our comparison is small relative to the variability of E and K among landscapes.

4. Methods

To test predictions of our relief-denudation relationship in our two study sites, we must estimate characteristic

hillslope lengths. This is accomplished by considering the typical particle transport distance on slopes. In other words, if we were able to distribute particles along the drainage divides in our study area, how far would they travel (measured horizontally) before entering the valley network? This approach accounts for the combined influence of planform and profile topographic variations that are typical of real hillslopes, yet enables us to apply the one-dimensional formulation developed above to real landscapes represented by two-dimensional digital elevation models. We use a topography-based hydrologic model to approximate hillslope length using upslope contributing area per unit contour width (a/b) (Costa-Cabral and Burges, 1994). Plots of $\log(a/b)$ versus local gradient typically exhibit a 'boomerang' shape whereby the lower arm defines how slope increases with a/b on hillslopes and the other arm shows decreasing valley slope angles with increasing a/b. In other words, on hillslopes, slope increases monotonically in the downslope direction (as a/b increases) attaining a maximum value just before entering the valley network. Once in the valley network, slope decreases in the down-valley direction (increasing a/b) consistent with the concavity of most valley profiles. The transition between these two regimes, which can be estimated by fitting a continuous function to the data and finding the maximum, defines the characteristic hillslope length. To estimate the representative hillslope length, we fit spline curves to topographic gradient as a function of $\log(a/b)$. We then determined the a/b value associated with the maximum predicted gradient value, thereby defining the kink in the 'boomerang' that corresponds to the characteristic hillslope length, L_H. We used two different approaches to measure L_H (constructing binned

averages of $\log(a/b)$ data to find the maximum gradient, and using a spline curve to the define the kink).

In contrast to previous studies that difference the maximum and minimum elevation within a fixed-radius moving window to estimate the distribution of local relief, we estimated average hillslope relief for each study site by setting the diameter of the moving window to the characteristic hillslope length, L_H, for that study site. This approach enables us to isolate the contribution of hillslopes to the total relief of the landscape and test the hillslope relief predictions of our model (Eq. (10)). Finally, in estimating the distribution of hillslope gradients, we limit our analysis to nonconvergent topography ($d^2z/dx^2 \leq 0$), such that portions of the valley network are excluded.

5. Results

Plots of a/b versus gradient for our two study sites reveal a 'boomerang' pattern delineating zones driven by hillslope and valley-forming processes (Fig. 4). For both sites, gradient increases with a/b, attaining a maximum value and then decreasing systematically for a/b values greater than ~ 100 m. The data defining these trends are less variable for hillslopes than for the valley network, possibly signaling the episodicity of valley-forming processes (e.g., debris flows in OCR and gullying in GM). Values of representative hillslope length (L_H) for the OCR and GM study areas are 57 and 72 m, respectively. Shorter hillslope lengths in the OCR are consistent with the high density of topographic hollows found along the upper tips of the valley network.

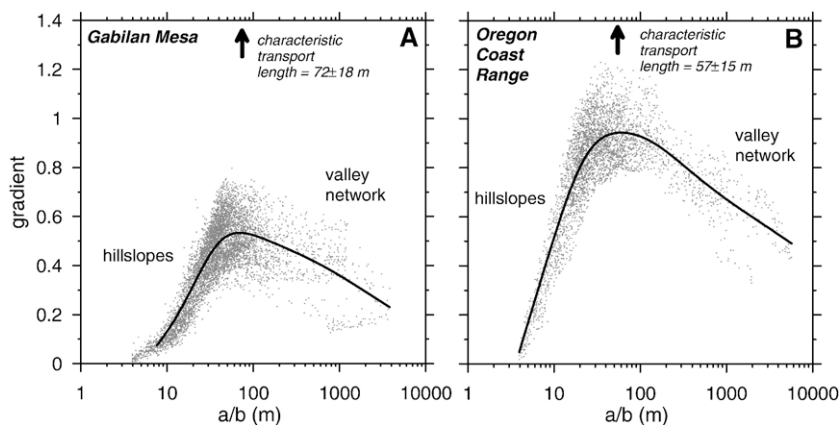Estimation of dimensionless relief (R^*) values enables us to quantify the degree to which nonlinear transport

Fig. 4. Semi-log plot of drainage area per unit contour width (a/b) and local gradient of the GM (A) and OCR (B) study sites. Low a/b values correspond to hilltops or drainage divides. Slope angles increase with a/b, reaching a maximum near the hillslope-valley transition. In the valley network, slope gradients decrease systematically with increasing a/b, thereby defining the concavity of valley profiles. a/b values associated with the maximum gradient values are used to define the characteristic hillslope length. We used spline curves (bold lines) fit to the data to find the maximum gradient value for a particular value of a/b. GM slopes are gentler and longer than typical OCR slopes.

Table 1
Study site summary statistics and model predictions

	Oregon Coast Range	Gabilan Mesa
K, transport coefficient [a] (m^2 yr^{-1})	0.003 ± 0.0005	$0.038 + 0.040/-0.024$
S_c, critical gradient [a]	1.2 ± 0.1	1.2 ± 0.4
E, erosion rate [b] (mm yr^{-1})	0.1 ± 0.05	$0.36 + 0.38/-0.22$
ρ_r/ρ_s, ratio of rock-to-soil bulk density	2.0	1.5
L_H, characteristic hillslope length (m) (see Fig. 4)	57 ± 15	72 ± 18
C_{HT}, hilltop curvature (m^{-1}) ($\pm$S.D.)	-0.07 ± 0.008	-0.014 ± 0.003
E^*, dimensionless erosion rate	6.3 ± 2.1	1.68 ± 0.70
S, Average gradient, predicted using Eq. (10)	0.78	0.40
S, Average gradient ($\pm$S.D.), (measured see Fig. 5A)	0.77 ± 0.20	0.41 ± 0.15
Relief (m), predicted using Eq. (10)	44	29
Relief (m), average $\pm$ S.D. (measured, see Fig. 5B)	39 ± 11	37 ± 7
R^*, dimensionless relief, predicted using Eq. (10), $R^* = f(E^*)$	0.65 ± 0.2	0.33 ± 0.19
R^*, dimensionless relief, Eq. (10), $R^* = S/S_c$ (measured using S)	0.64 ± 0.18	0.34 ± 0.17
R^*, dimensionless relief, Eq. (10), $R^* = R/L_H S_c$ (measured using R, L_H)	0.57 ± 0.23	0.43 ± 0.20

All errors are standard errors of the mean unless otherwise indicated.
[a] (Roering et al., 1999; Perron et al., 2005).
[b] (Heimsath et al., 2001; Bierman et al., 2001; Perron et al., 2005; Perron, 2006).

processes modulate slope morphology and the extent of denudation-relief coupling. Values of E^* for the OCR and GM sites are 6.33 and 1.68, yielding *predicted R** values (calculated using Eq. (10) where $R^* = f(E^*)$) of 0.65 and 0.33, respectively (Table 1). In addition, we can estimate R^* values for our two sites using readily obtained topographic information and the relations: $R^* = S/S_c$ and $R^* = R/(L_H S_c)$. These two equations yield 0.64 and 0.57, for our Oregon Coast Range site, and 0.34 and 0.43 for the Gabilan Mesa site, respectively (Fig. 2). These values of R^* are similar to those predicted using $R^* = f(E^*)$. Higher R^* values in the OCR are consistent with the visual perception that slopes in the OCR are steeper and thus less sensitive to increases in erosion rate than GM slopes (Fig. 2). The broad

convexity of GM slopes suggests that morphologic adjustments induced by changes in the transport coefficient κ or the rate of baselevel lowering E would result in proportional changes in average slope and relief. By contrast, because the OCR's R^* value is positioned along the cusp of the relief-denudation curve, its hillslope morphology will be less responsive to changes in K or E. As Eq. (10) indicates, when steady-state average hillslope gradients approach S_c, increases in baselevel lowering will foster only minor increases in average slope and relief.

Hillslope gradients estimated for the OCR study site are measurably steeper than those in the GM (Fig. 5A), although the local relief distributions for the two sites cannot be easily distinguished (Fig. 5B). This observation
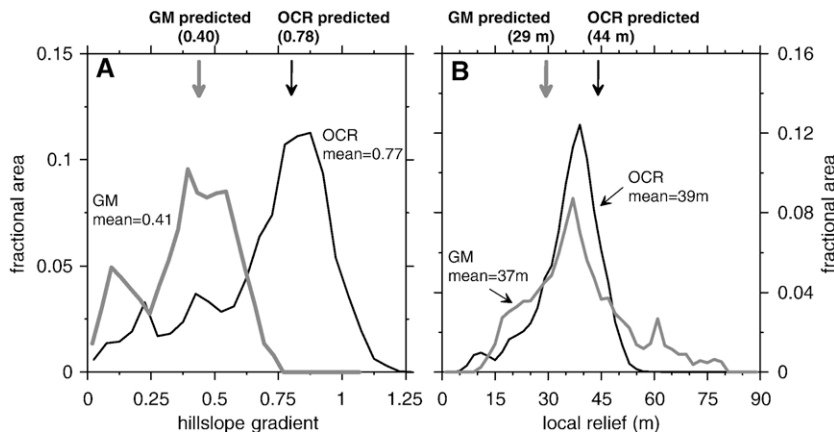

Fig. 5. Frequency plots of average hillslope gradient (A) and local relief (B) for the GM and OCR study areas. Gradient values for both sites were measured using a 4-m grid derived via airborne LiDAR. Local relief values reflect relief associated with hillslopes and are calculated as the elevation range within a moving window whose diameter is set to the characteristic hillslope length, L_H, for each site. For the OCR, $L_H = 57$ m and for the GM, $L_H = 72$ m. The sites have similar hillslope relief because OCR slopes are steeper and shorter than their GM counterparts.

emphasizes that local relief alone may not be sufficient to distinguish landscapes with different degrees of erosion-topography coupling (Fig. 2). Consistent with our analysis of $R*$ values described above, values of average gradient and representative hillslope relief predicted using Eq. (10) ($S=R*S_c$ and $R=R*S_cL_H$) compare well with these observations (Fig. 2). Predicted values for average slope angle are 0.78 and 0.40 for the OCR and GM sites (Table 1), consistent with the measured values of 0.77 and 0.41, respectively, (estimated from the distributions shown in Fig. 5A). For the OCR site, our equations for R and S slightly over-predict local relief; the predicted value is 44 m and the observed average value is 39 m. For the GM site, our equations slightly under-predict local relief; the predicted and observed values are 29 and 37 m, respectively (Fig. 5B).

6. Discussion

Our framework for analyzing how climatic and tectonic forcing affect landscape form depends on the steady-state assumption. Because changes in baselevel lowering are transmitted to hillslopes via channel incision, the realization of a steady-state relief structure depends on the response timescales of both the channel network and hillslopes (Mudd and Furbish, 2005; Roering et al., 2001b; Whipple and Tucker, 1999). Climatic variations likely affect hillslope transport parameters, although the functional relationships and thus response timescales remain poorly defined. Nonetheless, given sufficient justification for approximate steady-state conditions, our formulation provides a simple and efficient means of estimating topographic relief at the hillslope scale. This contribution may prove particularly useful for regional-scale landscape simulations that use coarse (>50 m) grid cells (Roe et al., 2003; Willett, 1999). For example, if the necessary suite of hillslope parameters can be defined, Eq. (10) enables the calculation of hillslope relief, obviating the need to explicitly model the evolution of individual hillslopes.

Our formulation could serve as one component of a relief-denudation analysis whereby the relief associated with various process domains is superimposed to estimate range-scale relief (Stock and Dietrich, 2003; Whipple et al., 1999). For example, by combining our hillslope formulation with a model for debris flows and fluvial relief, one could construct an analytical, range-scale denudation-relief equation to predict how changes in climate may influence landscape dynamics (Whipple et al., 1999). Such an approach complements empirical studies that use erosion rates and relief estimated across entire watersheds to deduce topography-denudation relationships (Montgomery and Brandon, 2002; Binnie et al., 2007). Limits to topographic development identified by previous studies have been suggested to depend on climate, lithology, and other factors that modulate the suite of geomorphic processes occurring in mountainous regions (Montgomery and Brandon, 2002; Burbank et al., 1996; Schmidt and Montgomery, 1995; Hutchinson, 1967; Kirkby, 1984; Gabet et al., 2004). Given the diverse processes and properties persistent in mountainous landscapes, it is unclear whether a substantial degree of generality should relate orogen-scale relief and denudation rate.

Our hillslope morphology-denudation relationships are derived from a one-dimensional analysis in order to make the analysis tractable and to eliminate the need for additional parameters to describe planform curvature. Real landscapes feature both planform and profile curvature, of which our approach only accounts for the latter. Nonetheless, previous landscape evolution studies comparing results from one-dimensional analytical solutions with two-dimensional numerical models conclude that one-dimensional formulations can produce meaningful results. Howard (1997) compared landscape evolution simulations using hillslope and fluvial transport models and demonstrated that one-dimensional simulations capture similar characteristics as their two-dimensional counterparts. More recently, Lave (2005) explored predictions of detachment-limited process models and demonstrated that a 1-D analytical solution for mean watershed elevation compared well with numerical 2-D surface evolution simulations. Because drainage density depends strongly on the chosen model for valley incision via fluvial, debris flow, or other processes, one can not use a two-dimensional model to isolate the role of hillslope processes (Howard, 1997). The fact that our predicted values of hillslope relief deviate from observed values (Fig. 5B) may reflect the varying influence of planform and profile curvature at our OCR and GM study sites. In the OCR, planform curvature predominates as profile curvature is typically limited to drainage divides or hilltops (Fig. 3). Hillslopes in the Gabilan Mesa site, on the other hand, exhibit a higher relative proportion of profile curvature.

The sensitivity of the relief-denudation coupling can be assessed from the nondimensional relief number $R*$, which can be easily evaluated from the average slope and S_c. The high values of $R*$ obtained for the steep, nearly planar slopes of the OCR ($R*=S/S_c=0.64$) imply that increases in erosion rate will result in marginal increases in relief and hillslope gradient (Fig. 2). In contrast, GM hillslopes are broadly convex with little topographic manifestation of nonlinear transport processes (Eq. (1)).

The $R*$ for the GM site, however, lies below the cusp of significant curvature in the $R*$–$E*$ relationship (Fig. 2). As a result, our formulation predicts that even slight increases in erosion rate or slope length will result in a morphologic adjustment. Similar morphologic changes could also occur through changes in K, which may result from climate-driven changes in disturbance-driven transport processes via biogenic processes (such as tree turnover or mammal burrowing (Yoo et al., 2005)). Our results are consistent with previous empirical findings that demonstrate a continuous transition between the "sub-threshold/threshold" and "transport-limited/detachment-limited" regimes quantified by Montgomery and Brandon (2002) and Binnie et al. (2007), respectively.

Interestingly, our two study sites exhibit similar distributions of hillslope relief, despite their disparate gradient distributions and $R*$ values. This coincidence in relief values arises because slopes are 25% longer in the GM than in the OCR, providing a broader platform on which hillslope relief can be constructed. This correspondence, furthermore, emphasizes the notion that hillslopes with similar relief (measured crest-to-channel) can exhibit very different morphologies as well as sensitivities to tectonic and/or climatic forcing (as quantified by $R*$).

The contribution of average hillslope relief to watershed relief (after normalizing for watershed size) also varies significantly between our two study sites. In both of our study sites, we selected similar-sized catchments, each including two second-order channels as well as the intervening ridgelines. This enabled us to characterize the broader relief structure including that associated with hillslopes and the low-order valley system (Fig. 3). In the OCR, total catchment relief for the region surrounding our study site is 380 m, whereas in the GM site, total relief is only 120 m. Thus, hillslopes comprise ∼10% of total relief in the OCR and 30–35% in GM. In both areas, relief carried by the valley network constitutes most of the range-scale topographic development. Shallow landsliding and overland flow erosion likely maintain valleys in the OCR and GM sites, respectively, and models have been proposed for quantifying how these processes contribute to the development of mountainous topography (Stock and Dietrich, 2006).

The delineation of hillslope-valley transitions as illustrated in our $\log(a/b)$-gradient analyses (Fig. 4) requires high-resolution topographic data like that provided via airborne laser altimetry (Dietrich et al., 2003). Coarser topographic data are typically insufficient for distinguishing the topographic signature of hillslopes in sufficient detail, or for measuring their length scale (Montgomery and Foufoula-Georgiou, 1993; Dietrich and Montgomery, 1998). Our formulation for dimension-less relief requires constraints on erosion rate E, hillslope length L_H, and transport parameters (K and S_c) or alternatively hilltop curvature C_{HT}, slope length L_H, and the critical slope parameter S_c. The analysis of cosmogenic radionuclides in stream sediments has revolutionized our ability to estimate long-term (>1000 yr), catchment-averaged erosion rates in mountainous landscapes (Granger et al., 1996), facilitating the application of our denudation-relief model.

The equation $R*=S/S_c$ provides a simple means to quantify sensitivity to changes in erosion rates or climate (which could include either transport coefficient, K or S_c). If $R*$ is large (near 1), then relief (for a given L_H is insensitive to K or E, but is sensitive to S_c. If $R*$ is small, then relief is insensitive to S_c, but sensitive to K and E. Certainly, the validity of these predictions depends on the validity of our nonlinear transport model and the applicability of steady state conditions in natural landscapes. The $E*$–$R*$ curve (Fig. 2) is a single universal curve for the nonlinear model such that any steady state hillslope will plot along the curve. Accordingly, the $E*$–$R*$ curve can be used to test the extent to which natural landscapes conform to our theory.

The model developed here assumes transport-limited conditions such that soil production rates are able to keep pace with erosion rates. Certainly this balance breaks down when erosion exceeds soil production, leading to bedrock exposure and a different suite of sediment production processes (Selby, 1993). At high $R*$ values (Fig. 2), accelerated transport via mass wasting may occur, potentially generating a production-erosion imbalance. Biogenic-driven disturbances responsible for dispersing and transporting soil, for example, may be outpaced by baselevel lowering such that soils are stripped. Although soil production functions have been quantified and calibrated at several locations globally (Heimsath et al., 2001, 2000; Heimsath, 1999; Wilkinson and Humphreys, 2005), functional relationships between soil production parameters and controlling factors such as lithology, vegetation, and climate remain unclear. Empirical evidence suggests that regions with coherent bedrock and erosion rates greater than 0.5 mm yr^{-1} tend to exhibit patchy and discontinuous soil mantles (Whipple et al., 2005). Our analysis may provide a quantitative framework for understanding the transition from soil-mantled landscapes to bedrock slopes. In our OCR study site, for example, maximum soil production rates (0.27 mm yr^{-1}) are more than twice the erosion rate used here, corresponding to an $R*$ value of ∼0.8. Not surprisingly, this corresponds to a point along our relief-denudation curve ($E*$=15.5, $R*$=0.8) where relief and erosion rates are only weakly coupled.

7. Conclusions

Our results provide a simplified framework for calculating hillslope profiles of elevation, slope, and curvature, from values of the transport parameters K and S_c and the erosion rate E. The reference erosion rate E_R defined here serves to distinguish the conditions for which the nonlinearity in our sediment transport model affects slope morphology and sensitivity to various perturbations. The nondimensional equations derived here demonstrate that on hillslopes with sufficiently high erosion rates, slope gradients become increasingly uniform and approach the critical value for which fluxes would become infinite. The profiles of such hillslopes become increasingly planar, consistent with previously proposed threshold slope models. Predicted values of hillslope gradient and relief compare well with topographic analyses from our two study sites in the Oregon Coast Range (OCR) and Gabilan Mesa, California (GM). According to the model, OCR slopes are poised along the cusp of the relief-erosion curve such that increases in erosion rate would produce marginal increases in gradient and relief. In contrast, GM slopes are situated on the steep part of the relief-erosion curve, such that relief and gradient are highly sensitive to erosion rate changes. Our results may serve as a building block in constructing process-based relief-denudation relationships and also should be useful for representing sub-grid scale topography in coarse-scale landscape evolution models.

Acknowledgments

References

Aalto, R., Dunne, T., Guyot, J.L., 2006. Geomorphic controls on Andean denudation rates. J. Geol. 114 (1), 85–99.

Ahnert, F., 1970. Functional relationships between denudation, relief and uplift in large, mid-latitude drainage basins. Am. J. Sci. 268, 243–263.

Anderson, R.S., 1994. Evolution of the Santa Cruz Mountains, California, through tectonic growth and geomorphic decay. J. Geophys. Res. 99 (10), 20,161–20,174.

Andrews, D.J., Bucknam, R.C., 1987. Fitting degradation of shoreline scarps by a nonlinear diffusion model. J. Geophys. Res. 92, 12,857–12,867.

Baldwin, E.M., 1956. Geologic map of the lower Siuslaw River area, Oregon. United States Geological Survey, Oil and Gas Invest. Map OM-186.

Benda, L., Dunne, T., 1997. Stochastic forcing of sediment supply to channel networks from landsliding and debris flow. Water Resour. Res. 33 (12), 2849–2863.

Bierman, P., Clapp, E., Nichols, K., Gillespie, A., Caffee, M., 2001. Using cosmogenic nuclide measurements in sediments to understand background rates of erosion and sediment transport. In: Harmon, Doe (Eds.), Landscape Erosion and Evolution Modeling. Kluwer Academic Plenum, New York, pp. 89–115.

Beschta, R.L., 1978. Long-term patterns of sediment production following road construction and logging in the Oregon Coast Range. Water Resour. Res. 14, 1011–1016.

Binnie, S., Phillips, W., Summerfield, M.A., Fifield, L., 2007. Tectonic uplift, threshold hillslopes, and denudation rates in a developing mountain range. Geology 35 (8), 743–746.

Burbank, D.W., Leland, J., Fielding, E., Anderson, R.S., Brozovic, N., Reid, M.R., Duncan, C., 1996. Bedrock incision, rock uplift and threshold hillslopes in the Northwestern Himalayas. Nature 379 (6565), 505–510.

Carson, M.A., 1976. Mass-wasting, slope development, and climate. In: Derbyshire, E. (Ed.), Geomorphology and Climate. John Wiley and Sons, New York, pp. 101–136.

Carson, M.A., Petley, D.J., 1970. The existence of threshold hillslopes in the denudation of the landscape. Trans. Inst. Brit. Geog. 49, 71–95.

Costa-Cabral, M.C., Burges, S.J., 1994. Digital elevation model networks (DEMON): a model of flow over hillslopes for computation of contributing and dispersal areas. Water Resour. Res. 30, 1681–1692.

Dibblee, T.W., 1979. Cenozoic tectonics of the northeast flank of the Santa Lucia Mountains from the Arroyo Seco to the Nacimiento River, California. In: Graham, S.A. (Ed.), Tertiary and Quaternary Geology of the Salinas Valley and Santa Lucia Range, Monterey County, California. Pacific Coast Paleogeography Field Guide, vol. 4. SEPM, pp. 67–76.

Dietrich, W.E., Dunne, T., 1978. Sediment budget for a small catchment in mountainous terrain. Z. Geomorphol., Suppl. 29, 191–206.

Dietrich, W.E., Montgomery, D.R., 1998. Hillslopes, channels, and landscape scale. In: Sposito, G. (Ed.), Scale Dependence and Scale Invariance in Hydrology. Cambridge University Press, Cambridge, pp. 30–60.

Dietrich, W.E., Bellugi, D., Sklar, L.S., Stock, J.D., Heimsath, A.M., Roering, J.J., 2003. Geomorphic transport laws for predicting landscape form and dynamics. In: Iverson, R.M., Wilcock, P. (Eds.), Prediction in Geomorphology. American Geophysical Union, Washington, D.C., pp. 103–132.

Dohrenwend, J.C., 1979a. Provenance and paleodrainage of the northern part of the Paso Robles Formation, Monterey County, California. In: Graham, S.A. (Ed.), Tertiary and Quaternary Geology of the Salinas Valley and Santa Lucia Range, Monterey County, California. Pacific Coast Paleogeography Field Guide, vol. 4. SEPM, pp. 77–82.

Dohrenwend, J.C., 1979b. Morphologic analysis of Gabilan Mesa by iterative contour generalization: An improved method of geomorphic cartographic analysis. In: Graham, S.A. (Ed.), Tertiary and Quaternary Geology of the Salinas Valley and Santa Lucia Range,

Monterey County, California. Pacific Coast Paleogeography Field Guide, vol. 4. SEPM, pp. 83–88.

Durham, D.L., 1974. Geology of the southern Salinas Valley area, California, US. Geol. Surv. Prof. Pap. 819, 111.

Freeze, R.A., 1987. Modelling interrelationships between climate, hydrology, and hydrogeology and the development of slopes. In: Anderson, M.G., Richard, K.S. (Eds.), Slope Stability. Wiley & Sons, Chichester, pp. 381–403.

Furbish, D.J., Fagherazzi, S., 2001. Stability of creeping soil and implications for hillslope evolution. Water Resour. Res. 37, 2607–2618.

Gabet, E.J., 2000. Gopher bioturbation: field evidence for non-linear hillslope diffusion. Earth Surf. Processes Landf. 25 (13), 1419–1428.

Gabet, E.J., 2003. Sediment transport by dry ravel. J. Geophys. Res.— Solid Earth 108 (B1), doi:10.1029/2001JB001686.

Gabet, E.J., Pratt-Sitaula, B.A., Burbank, D.W., 2004. Climatic controls on hillslope angle and relief in the Himalayas. Geology 32 (7), 629–632.

Galehouse, J.S., 1967. Provenance and paleocurrents of the Paso Robles Formation, California. Bull. Geol. Soc. Am. 78 (8), 951–978.

Granger, D.E., Kirchner, J.W., Finkel, R., 1996. Spatially averaged long-term erosion rates measured from in-situ produced cosmogenic nuclides in alluvial sediment. J. Geol. 104 (3), 249–257.

Heimsath, A.M., 1999. The Soil Production Function, Ph.D. University of California, Berkeley.

Heimsath, A.M., Chappell, J., Dietrich, W.E., Nishiizumi, K., Finkel, R.C., 2000. Soil production on a retreating escarpment in southeastern Australia. Geology 28 (9), 787–790.

Heimsath, A.M., Dietrich, W.E., Nishiizumi, K., Finkel, R.C., 2001. Stochastic processes of soil production and transport: erosion rates, topographic variation and cosmogenic nuclides in the Oregon Coast Range. Earth Surf. Processes Landf. 26 (5), 531–552.

Heimsath, A.M., Furbish, D.J., Dietrich, W.E., 2005. The illusion of diffusion: field evidence for depth-dependent sediment transport. Geology 33 (12), 949–952.

Howard, A.D., 1994. A detachment-limited model of drainage basin evolution. Water Resour. Res. 30 (7), 2261–2285.

Howard, A.D., 1997. Badland morphology and evolution: interpretation using a simulation model. Earth Surf. Processes Landf. 22, 211–227.

Hutchinson, J.N., 1967. The free degradation of the London clay cliffs. Proceedings, Geotechnical Conference of Oslo, vol. 1, pp. 113–118.

Kelsey, H.M., Ticknor, R.L., Bockheim, J.G., Mitchell, C.E., 1996. Quaternary upper plate deformation in coastal Oregon. Geol. Soc. Amer. Bull. 108 (7), 843–860.

Kirkby, M.J., 1984. Modelling cliff development in South Wales; Savigear re-reviewed. Z. Geomorphol. 28 (4), 405–426.

Lave, J., 2005. Analytic solution of the mean elevation of a watershed dominated by fluvial incision and hillslope landslides. Geophys. Res. Lett. 32 (11).

Milliman, J.D., Meade, R.H., 1983. World-wide delivery of river sediment to the oceans. J. Geol. 91 (1), 1–21.

Milliman, J.D., Syvitski, J.P.M., 1992. Geomorphic/tectonic control of sediment discharge to the ocean: the importance of small mountainous rivers. J. Geol. 100, 525–544.

Montgomery, D.R., 2001. Slope distributions, threshold hillslopes, and steady-state topography. Am. J. Sci. 301 (4–5), 432–454.

Montgomery, D.R., Foufoula-Georgiou, E., 1993. Channel networks sources representation using digital elevation models. Water Resour. Res. 29, 1925–1934.

Montgomery, D.R., Brandon, M.T., 2002. Topographic controls on erosion rates in tectonically active mountain ranges. Earth Planet. Sci. Lett. 201, 481–489.

Montgomery, D.R., Schmidt, K.M., Greenberg, H., Dietrich, W.E., 2000. Forest clearing and regional landsliding. Geology 28, 311–314.

Mudd, S.M., Furbish, D.J., 2005. Lateral migration of hillcrests in response to channel incision in soil-mantled landscapes. J. Geophys. Res.—Earth Surface 110 (F4).

Orr, E.L., Orr, W.N., Baldwin, E.M., 1992. Geology of Oregon. Kendall/Hunt Pub Co., Dubuque. 254 pp.

Penck, W., 1953. Morphological Analysis of Landforms. MacMillian, London. 429 pp.

Perron, J.T., Formation of evenly spaced ridges and valleys, PhD thesis, University of California, Berkeley, 2006.

Perron, J.T., Kirchner, J.W., Dietrich, W.E., 2003. Measuring landscape scale and testing landscape evolution models with an airborne laser swath map of the Gabilan Mesa, California. AGU Fall Meet. Abstracts 12, 03.

Perron, J.T., Kirchner, J.W., Dietrich, W.E., Finkel, R.C., 2005. Testing Model Predictions of the Evolution of Valley Spacing. Fall Meeting. American Geophysical Union. abstract# H33F-02.

Personius, S.F., 1995. Late Quaternary stream incision and uplift in the forearc of the Cascadia subduction zone, western Oregon. J. Geophys. Res. 100, 20,193–20,210.

Pinet, P., Souriau, M., 1988. Continental erosion and large-scale relief. Tectonics 7, 563–582.

Reneau, S.L., Dietrich, W.E., 1990. Depositional history of hollows on steep hillslopes, coastal Oregon and Washington. Natl. Geogr. Res. 6 (2), 220–230.

Reneau, S.L., Dietrich, W.E., 1991. Erosion rates in the Southern Oregon Coast Range: evidence for an equilibrium between hillslope erosion and sediment yield. Earth Surf. Processes Landf. 16 (4), 307–322.

Roe, G.H., Montgomery, D.R., Hallet, B., 2003. Orographic precipitation and the relief of mountain ranges. J. Geophys. Res.—Solid Earth 108 (B6, Art. No. 2315).

Roering, J., 2006. How well can hillslope evolution models explain real topography? Geological Society of America, Annual Meeting, vol. 38. GSA, Philadelphia, PA, p. 174.

Roering, J.J., Gerber, M., 2005. Fire and the evolution of steep, soil-mantled landscapes. Geology 33 (5), 349–352.

Roering, J.J., Kirchner, J.W., Dietrich, W.E., 1999. Evidence for nonlinear, diffusive sediment transport on hillslopes and implications for landscape morphology. Water Resour. Res. 35 (3), 853–870.

Roering, J.J., Kirchner, J.W., Sklar, L.S., Dietrich, W.E., 2001a. Hillslope evolution by nonlinear creep and landsliding: an experimental study. Geology 29, 143–146.

Roering, J.J., Kirchner, J.W., Dietrich, W.E., 2001b. Hillslope evolution by nonlinear, slope-dependent transport: steady-state morphology and equilibrium adjustment timescales. J. Geophys. Res. 106 (B8), 16,499–16,513.

Roering, J.J., Kirchner, J.W., Dietrich, W.E., 2005. Characterizing structural and lithologic controls on deep-seatedlandsliding: implications for topographic relief and landscape evolution in the Oregon Coast Range, USA. Geol. Soc. Amer. Bull. 117 (5/6), 654–668.

Schmidt, K.M., 1999. Root Strength, Colluvial Soil Depth, and Colluvial Transport on Landslide-prone Hillslopes, Ph.D. University of Washington.

Schmidt, K.M., Montgomery, D.R., 1995. Limits to relief. Science 270, 617–620.

Selby, M.J., 1993. Hillslope Materials and Processes. Oxford Univ. Press, Oxford. 451 pp.

Snavely, P.D., Wagner, H.C., N.S. MacLeod, 1964. Rhythmic-bedded eugeosynclinal deposits of the Tyee Formation, Oregon Coast Range, Kansas. Geol. Surv. Bull. 169, 461–480.

Stock, J., Dietrich, W.E., 2003. Valley incision by debris flows: evidence of a topographic signature. Water Resour. Res. 39 (4, art. no. 1089).

Stock, J., Dietrich, W., 2006. Erosion of steepland valleys by debris flows. Geol. Soc. Amer. Bull. 118 (9), 1125–1148.

Strahler, A.N., 1950. Equilibrium theory of erosional slopes approached by frequency distribution analysis. Am. J. Sci. 248, 673–696.

Summerfield, M.A., Nulton, N.J., 1994. Natural controls of fluvial denudation rates in major world drainage basin. J. Geophys. Res. 99 (7), 13,871–13,883.

Whipple, K.X., Tucker, G.E., 1999. Dynamics of the stream-power river incision model: implications for height limits of mountain ranges, landscape response timescales, and research needs. J. Geophys. Res. 104, 17,661–17,674.

Whipple, K.X., Kirby, E., Brocklehurst, S.H., 1999. Geomorphic limits to climate-induced increases in topographic relief. Nature 401, 39–43.

Whipple, K., Heimsath, A., Ouimet, W., Crosby, B., Wobus, C., 2005. The relation between topography and millennial erosion rates in the San Gabriel Mountains, California. Eos, Trans. AGU 86.

Wilkinson, M.T., Humphreys, G.S., 2005. Exploring pedogenesis via nuclide-based soil production rates and OSL-based bioturbation rates. Aust. J. Soil Res. 43 (6), 767–779.

Willett, S.D., 1999. Orogeny and orography: the effects of erosion on the structure of mountain belts. J. Geophys. Res.—Solid Earth 104 (B12), 28957–28981.

Yoo, K., Amundson, R., Heimsath, A.M., Dietrich, W.E., 2005. Process-based model linking pocket gopher (*Thomomys bottae*) activity to sediment transport and soil thickness. Geology 33 (11), 917–920.